Supplementary Material

Chaos in conservative discrete-time systems subjected to parameter drift

Dániel Jánosi, Tamás Tél

S1 A more general non-autonomous map and comparison with the simpler one

S1.a Ball remaining on the same slope

Two cases are considered depending on whether the ball hits the same slope on which it starts, or not; let us begin with the first one. According to the laws of oblique projection, the relation between the data of the nth and right before the $n+1$th collisions in orthogonal coordinates are

$$x_{n+1} = x_n + v_{x,n}t_n, \qquad y_{n+1} = y_n + v_{y,n}t_n - \frac{g}{2}t_n^2,$$
$$v_{x,n+1} = v_{x,n}, \qquad v_{y,n+1} = v_{y,n} - gt_n,$$

where t_n denotes the flight time. As the slope changes during the flight from α_n to some α_{n+1}, the ratios of the position coordinates are (see Fig.2a):

$$\frac{y_n}{x_n} = \operatorname{tg}\alpha_n, \qquad \frac{y_{n+1}}{x_{n+1}} = \operatorname{tg}\alpha_{n+1}.$$

Substituting here the x and y coordinates, one obtains

$$x_n \operatorname{tg}\alpha_n + v_{y,n}t_n - \frac{g}{2}t_n^2 = x_n \operatorname{tg}\alpha_{n+1} + v_{x,n}t_n \operatorname{tg}\alpha_{n+1},$$

from which a quadratic equation is obtained for the flight time t_n:

$$\frac{g}{2}t_n^2 - (v_{y,n} - v_{x,n}\operatorname{tg}\alpha_{n+1})t_n - y_n\left(1 - \frac{\operatorname{tg}\alpha_{n+1}}{\operatorname{tg}\alpha_n}\right) = 0.$$

The solution is:

$$gt_n = v_{y,n} - v_{x,n}\operatorname{tg}\alpha_{n+1} + \sqrt{D_n},$$

where D_n is the discriminant:

$$D_n = (v_{y,n} - v_{x,n}\operatorname{tg}\alpha_{n+1})^2 + 2g\left(1 - \frac{\operatorname{tg}\alpha_{n+1}}{\operatorname{tg}\alpha_n}\right)y_n.$$

Expressing this with the mechanical energy $\varepsilon_n = gy_n + \frac{1}{2}(v_{x,n}^2 + v_{y,n}^2)$, where ε_n stands for the energy per mass at the nth bounce, we get

$$D_n = (v_{y,n} - v_{x,n}\operatorname{tg}\alpha_{n+1})^2 + 2\left(1 - \frac{\operatorname{tg}\alpha_{n+1}}{\operatorname{tg}\alpha_n}\right)\left(\varepsilon_n - \frac{1}{2}(v_{x,n}^2 + v_{y,n}^2)\right).$$

The velocity components parallel (u) and normal (w) to the slope are expressed as:

$$u_n = v_{x,n}\cos\alpha_n + v_{y,n}\sin\alpha_n, \quad w_n = -v_{x,n}\sin\alpha_n + v_{y,n}\cos\alpha_n.$$

The inverse transformation is similar, and similar relations hold for the $n+1$th collision as well. The components of the impact velocity are:

$$\begin{aligned}
\tilde{u}_{n+1} &= v_{x,n+1}\cos\alpha_{n+1} + v_{y,n+1}\sin\alpha_{n+1} = v_{x,n}\cos\alpha_{n+1} + (v_{y,n} - gt_n)\sin\alpha_{n+1} = \\
&= \frac{\cos\alpha_n}{\cos\alpha_{n+1}}u_n - \frac{\sin\alpha_n}{\cos\alpha_{n+1}}w_n - \sqrt{D_n}\sin\alpha_{n+1}, \\
\tilde{w}_{n+1} &= -v_{x,n+1}\sin\alpha_{n+1} + v_{y,n+1}\cos\alpha_{n+1} = -v_{x,n}\sin\alpha_{n+1} + (v_{y,n} - gt_n)\cos\alpha_{n+1} = \\
&= -\cos\alpha_{n+1}\sqrt{D_n}.
\end{aligned}$$

For elastic bounces the normal component just changes sign, while the parallel one does not change at all: $u_{n+1} = \tilde{u}_{n+1}$, $w_{n+1} = -\tilde{w}_{n+1}$. Assuming that the new angle α_{n+1} has set in before the bounce and it is thus fixed at the instant of the collision, the energy remains the same: $\varepsilon_n = \varepsilon$. In order to obtain an explicit expression for w_{n+1}, one has to express the discriminant D_n with components u_n, w_n. After rearrangements, we arrive at

$$\begin{aligned}
w_{n+1}^2 = &\left(\frac{1}{2}\cos^2\alpha_n \sin 2\alpha_{n+1}\operatorname{ctg}\alpha_n - \frac{1}{4}\sin 2\alpha_n \sin 2\alpha_{n+1} - \cos^2\alpha_n \cos 2\alpha_{n+1}\right)u_n^2 + \\
&+ \left(\sin 2\alpha_n \cos 2\alpha_{n+1} - \cos 2\alpha_n \sin 2\alpha_{n+1}\right)u_n w_n + \\
&+ \left(\frac{1}{2}\cos^2\alpha_n \operatorname{ctg}\alpha_n \sin 2\alpha_{n+1} + \frac{3}{4}\sin 2\alpha_n \sin 2\alpha_{n+1} - \sin^2\alpha_n \cos 2\alpha_{n+1}\right)w_n^2 + \\
&+ 2\left(\cos^2\alpha_{n+1} - \frac{1}{2}\sin 2\alpha_{n+1}\operatorname{ctg}\alpha_n\right)\varepsilon.
\end{aligned}$$

Dimensionless forms are obtained by measuring velocities in units of $\sqrt{2\varepsilon}$. With the new variable $z = w^2$ the mapping reads as:

$$\boxed{\begin{aligned}
u_{n+1} = &\frac{\cos\alpha_n}{\cos\alpha_{n+1}}u_n - \frac{\sin\alpha_n}{\cos\alpha_{n+1}}\sqrt{z_n} - \operatorname{tg}\alpha_{n+1}\sqrt{z_{n+1}} \\
z_{n+1} = &\left(\frac{1}{2}\cos^2\alpha_n \sin 2\alpha_{n+1}\operatorname{ctg}\alpha_n - \frac{1}{4}\sin 2\alpha_n \sin 2\alpha_{n+1} - \cos^2\alpha_n \cos 2\alpha_{n+1}\right)u_n^2 + \\
&+ \left(\sin 2\alpha_n \cos 2\alpha_{n+1} - \cos 2\alpha_n \sin 2\alpha_{n+1}\right)u_n\sqrt{z_n} + \\
&+ \left(\frac{1}{2}\cos^2\alpha_n \operatorname{ctg}\alpha_n \sin 2\alpha_{n+1} + \frac{3}{4}\sin 2\alpha_n \sin 2\alpha_{n+1} - \sin^2\alpha_n \cos 2\alpha_{n+1}\right)z_n + \\
&+ \cos^2\alpha_{n+1} - \frac{1}{2}\sin 2\alpha_{n+1}\operatorname{ctg}\alpha_n.
\end{aligned}} \tag{S1}$$

This from is valid as long as the y_{n+1} vertical coordinate of the next collision is positive, since a negative value would indicate a location below the vertex, which is impossible. From here condition

$$u_{n+1}^2 + z_{n+1} \le 1$$

follows. This is formally the same as the condition formulated below (1), but when expressed with the initial velocities u_n, z_n, it is much more complicated.

S1.b Ball jumping over to the other slope

Now consider the second case. Here, the governing equations are

$$\begin{aligned} x_{n+1} &= x_n + v_{x,n}t_n, & y_{n+1} &= y_n + v_{y,n}t_n - \frac{g}{2}t_n^2, \\ v_{x,n+1} &= v_{x,n}, & v_{y,n+1} &= v_{y,n} - gt_n, \\ \frac{y_n}{x_n} &= \operatorname{tg}\alpha_n, & \frac{y_{n+1}}{x_{n+1}} &= -\operatorname{tg}\alpha_{n+1}, \end{aligned}$$

where the upward direction is considered positive on the other slope, too (see Fig.2b). After substitution, a quadratic equation is obtained for t_n:

$$\frac{g}{2}t_n^2 - (v_{x,n}\operatorname{tg}\alpha_{n+1} + v_{y,n})t_n - y_n\left(1 + \frac{\operatorname{tg}\alpha_{n+1}}{\operatorname{tg}\alpha_n}\right) = 0,$$

whose solution is:

$$gt_n = v_{y,n} + v_{x,n}\operatorname{tg}\alpha_{n+1} + \sqrt{D_n},$$

where the discriminant D_n for this case reads as:

$$D_n = (v_{y,n} + v_{x,n}\operatorname{tg}\alpha_{n+1})^2 + 2\left(1 + \frac{\operatorname{tg}\alpha_{n+1}}{\operatorname{tg}\alpha_n}\right)\left(\varepsilon - \frac{1}{2}(v_{x,n}^2 + v_{y,n}^2)\right).$$

The transformation between slope-based parallel and normal velocity components has a similar form as in the previous section for both the nth and $n+1$th bounces. Using these, the impact velocities before the $n+1$th bounce are:

$$\begin{aligned} \tilde{u}_{n+1} &= -v_{x,n}\cos\alpha_{n+1} + (v_{y,n} - gt_n)\sin\alpha_{n+1} = -\frac{\cos\alpha_n}{\cos\alpha_{n+1}}u_n + \frac{\sin\alpha_n}{\cos\alpha_{n+1}}w_n - \sqrt{D_n}\sin\alpha_{n+1}, \\ \tilde{w}_{n+1} &= v_{x,n}\sin\alpha_{n+1} + (v_{y,n} - gt_n)\cos\alpha_{n+1} = -\sqrt{D_n}\cos\alpha_{n+1}. \end{aligned}$$

The velocity components right after the bounce are obtained as in the previous case: $u_{n+1} = \tilde{u}_{n+1}$, $w_{n+1} = -\tilde{w}_{n+1}$. After expressing discriminant D_n appearing in w_{n+1} with the appropriate components and using z rather than w, the dimensionless form of the full mapping for this second case is obtained as:

$$\begin{aligned} u_{n+1} &= -\frac{\cos\alpha_n}{\cos\alpha_{n+1}}u_n + \frac{\sin\alpha_n}{\cos\alpha_{n+1}}\sqrt{z_n} - \operatorname{tg}\alpha_{n+1}\sqrt{z_{n+1}} \\ z_{n+1} &= -\left(\frac{1}{2}\cos^2\alpha_n \operatorname{ctg}\alpha_n \sin 2\alpha_{n+1} - \frac{1}{4}\sin 2\alpha_n \sin 2\alpha_{n+1} + \cos^2\alpha_n \cos 2\alpha_{n+1}\right)u_n^2 + \\ &\quad + \left(\sin 2\alpha_n \cos 2\alpha_{n+1} + \cos 2\alpha_n \sin 2\alpha_{n+1}\right)u_n\sqrt{z_n} - \\ &\quad - \left(\frac{1}{2}\cos^2\alpha_n \operatorname{ctg}\alpha_n \sin 2\alpha_{n+1} + \frac{3}{4}\sin 2\alpha_n \sin 2\alpha_{n+1} + \sin^2\alpha_n \cos 2\alpha_{n+1}\right)z_n + \\ &\quad + \frac{1}{2}\sin 2\alpha_{n+1}\operatorname{ctg}\alpha_n + \cos^2\alpha_{n+1}. \end{aligned} \tag{S2}$$

Note that the new mapping (S1), (S2) is more complicated than (1), (2), but the similarity in their structure is much more evident here than earlier. In the limiting case of $\alpha_{n+1} = \alpha_n$ recursions (S1), (S2) go over into the stationary mapping (1), (2).

It is worth comparing the results of the new dynamics (S1), (S2) with that of the simpler non-autonomous mapping (1), (2) augmented with the time-dependent extension (6). Using the same scenario, the results in the end state show only minor differences as visible in Fig.S1.

This reinforces the view that the essential results are not influenced by the choice of the mapping, and thus the use of the simpler form is justified in the main text.

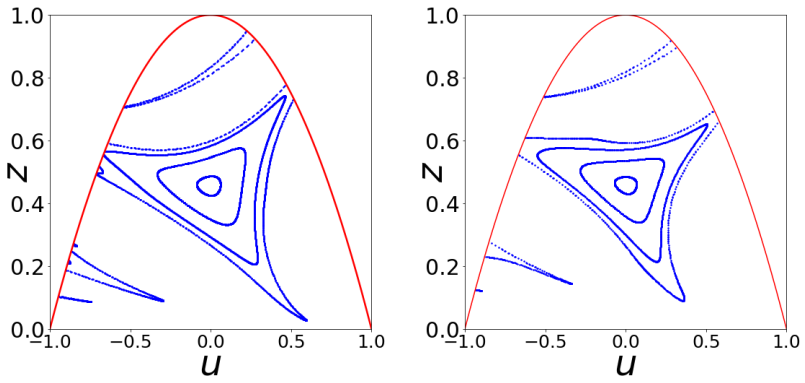

Figure S1: Phase portraits at the end of scenario $[70°, 50°, 10]$ with the simple mapping (1), (2), (6) used in the paper (a) and the more complex one (S1), (S2) (b). Initial conditions for the tori are: $z_0 = 0.4, 0.5, 0.6, 0.7$ and $u_0 = 0$ always.

S2 Standard map subjected to parameter drift

The physical origin of the standard map is a simplified, periodically kicked rotator. This can be pictured by considering a massless rod connected to a bob at one of its ends and to a rotating pole at the other, and while the system is in rotation, the bob is subjected to a periodic kicking. If the location dependence of this force is sinusoidal, then we call the resulting stroboscopic map the standard map which has the form

$$x_{n+1} = x_n + v_n, \qquad v_{n+1} = v_n + a \sin x_{n+1}, \tag{S3}$$

where x and v are the dimensionless arc length and peripheral velocity, while $a > 0$ is a dimensionless amplitude parameter. The phase portrait of the standard map for $a = 1$ can be seen in Fig.S2.

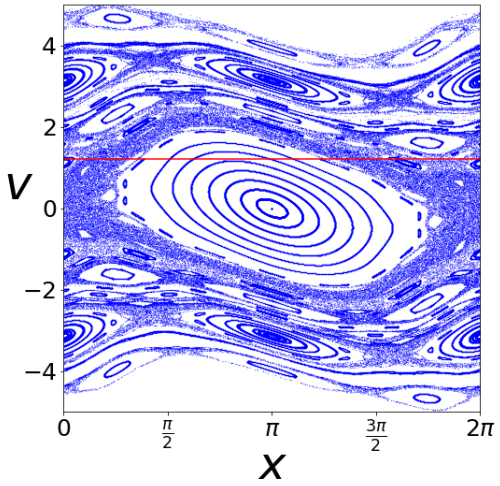

Figure S2: The phase space of the standard map with the amplitude parameter $a = 1$. Two sets of initial conditions were iterated 5000 times; 41 evenly spread points between -4 and 4 in v, with x values of 0 and π, respectively. The red line signals the value $v = 1.2$ and helps identifying the initial torus taken in Fig.S3.

We make this map non-autonomous the same way we did in the case of the symmetric wedge; we consider the switch

$$a \to a_n \tag{S4}$$

in (S3). We also define the scenario similarly; we consider a starting point a_0 and an endpoint a_f which is reached after N iterations in increments of $\Delta a = (a_f - a_0)/N$. The scenario is then denoted as $[a_0, a_f, N]$. The origin of the stationary phase space is a single hyperbolic fixed point, from which a snapshot hyperbolic point could evolve in the time-dependent system. This SHP, however, turns out to be nonmoving, (0,0) is a usual hyperbolic point during the whole scenario. We can also consider this as a stationary fixed point, and apply the method used in Section IV. The dynamical condition as formulated there corresponds to an instant n_c when some points of the tori first enter a close vicinity of the origin. There are no structural discontinuities in this system, thus we have no discontinuity condition to speak of in this case. Figure S3 shows that snapshot tori evolve similarly to those of the double wedge system; first they deform (Fig.S3a-S3b), then they break up (Fig.S3c, $n_c = 15$) and eventually their points spread out in the phase space (Fig.S3d), resulting in chaotic motion. Note, that in the spirit of Section VII, the origin can also be considered as an exactly known SHP, and therefore its stable manifold is an exact part of the pseudo-foliation of the snapshot chaotic sea.

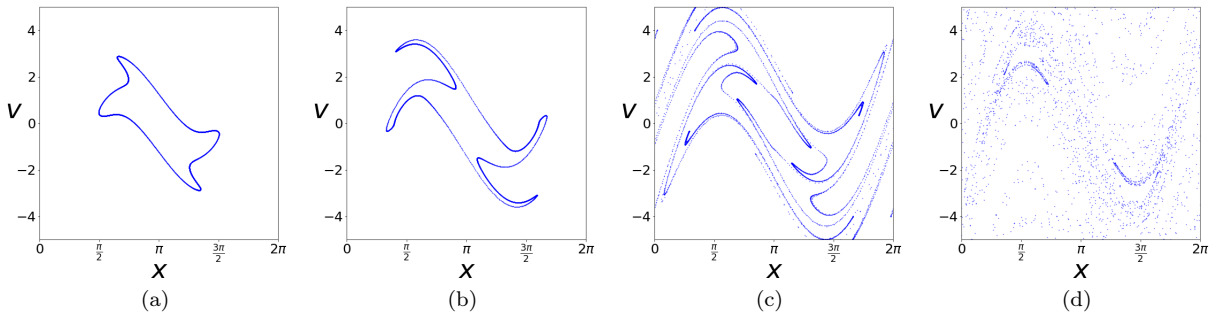

(a) (b) (c) (d)

Figure S3: The evolution of the snapshot torus of initial condition $x_0 = \pi$ and $v_0 = 1.2$ of the standard map (in Fig.S2, this torus is indicated by its crossing of the red line at $x = \pi$) according to the scenario [1, 6, 25]. The iteration numbers of the respective images are n = 10, 12, 15 and 25. It is apparent, that the break-up event happens on the third image, a few blue points are already in the vicinity of the origin, making the crossover time $n_c = 15$. At iteration number 25, the break up is complete, most of the blue dots are scattered in a chaotic region.

When monitoring the dynamical instability of the standard map, we apply the same method described in Section V of the main text, i.e. we calculate the EAPD quantity and the instantaneous Lyapunov exponent. Figure S4 shows the corresponding curves for two snapshot tori in the same scenario with their crossover times also indicated. Since the only thing differentiating between these curves is the initial location of the tori, we can conclude from the image that both the Lyapunov exponent and the crossover time for individual tori does indeed depend on their initial condition even in the same scenario.

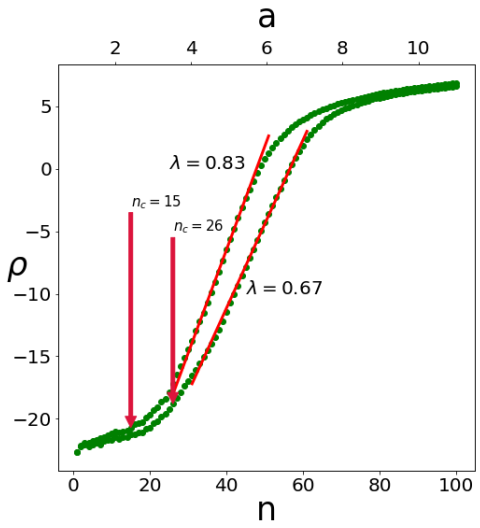

Figure S4: Dynamical instability of two snapshot tori of the standard map with the applied scenario being [1, 11, 100] in both cases. The initial condition of the torus of the upper curve is $x_0 = \pi$, $v_0 = 1.55$ (a large torus), while that of the lower one is $x_0 = \pi$, $v_0 = 0.8$ (a smaller torus). The crossover time and the Lyapunov exponent after torus break-up are found to be $n_c = 15$, $\lambda = 0.83$ and $n_c = 26$, $\lambda = 0.67$ in these cases. We see that both of these quantities depend on the chosen initial torus when the same scenario is applied.

S3 Supplementary figures

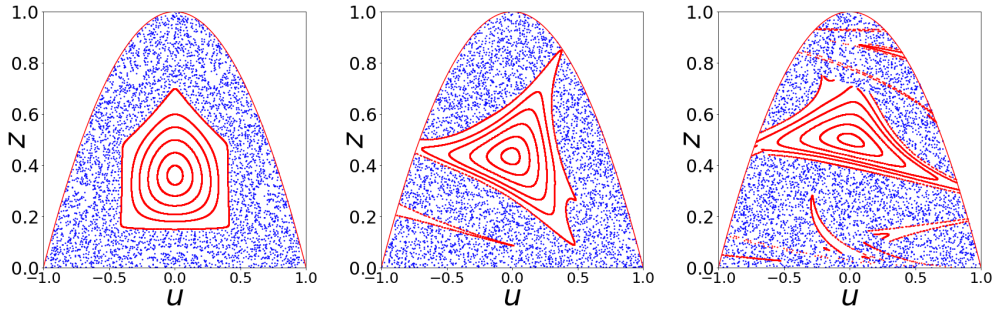

(a) (b) (c)

Figure S5: The evolution of the snapshot chaotic sea along with snapshot tori. Displayed are steps 0, 9, 13 of the scenario $[70°, 30°, 20]$ with initial conditions $z_0 = 0.9, 0.8, 0.7, 0.6, 0.55, 0.5, 0.45, 0.4$, the first two of which belong to the chaotic sea and $u_0 = 0$ for all. In panel (b) only the discontinuity condition is fulfilled and we can see that the snapshot chaotic sea does not enter the cut-off tendril, while in panel (c) the scenario is past the point of the dynamical condition as indicated by the several thin arcs. The general tendency is that white bands, here bounded by red torus pieces, originating from the quasi-periodic island are entrained into the chaotic sea.

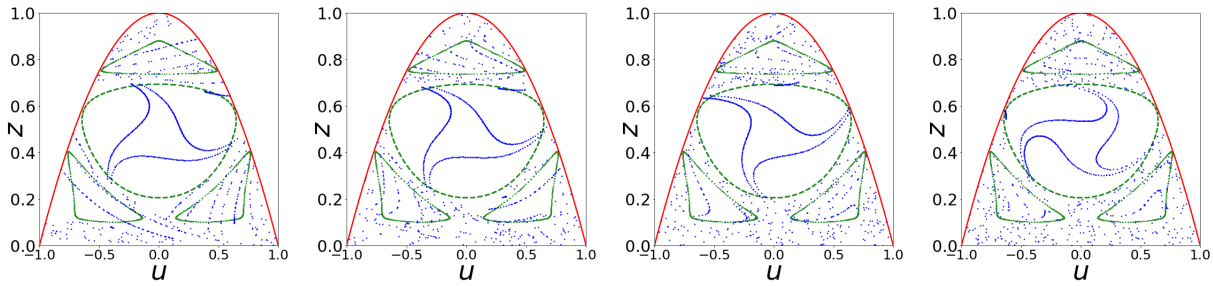

(a) (b) (c) (d)

Figure S6: Scenario ending on the plateau of $\alpha_p = 50°$, with the preceding scenario of $[70°, 50°, 40]$ with a torus smaller than in Fig.12 generated from the initial condition $u_0 = 0$, $z_0 = 0.55$. The images were taken at $n' = 0, 5, 15, 50$ steps on the plateau and the green boundary tori are the same as in Fig.12.

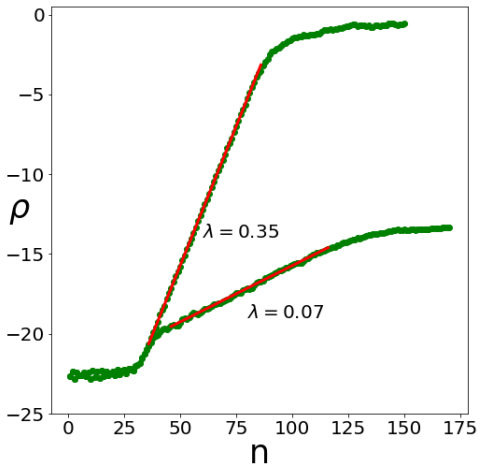

Figure S7: Dynamical instability in the plateau scenarios of Figures 11 (upper curve) and S6 (lower curve). The Lyapunov exponent is much smaller on the latter, but slightly larger than for the scenario of Fig.12 since more points of the original torus fall into the chaotic sea when arriving at the plateau in this case (compare with Fig.13).